Indian Journal of Pure & Applied Physics
Vol. 64, November 2026, pp. 1230-1236
DOI: 10.56042/ijpap.v64i11.32001

Design and Performance Investigation of Cylindrical Gate all around Junctionless Transistor for UV Photodetector Applications

Binay Binod Kumar[a*], Ankit Kumar Singh[b] & Kunal Singh[b]

[a]Department of Electronics and Communication Engineering, Siddhartha Academy of Higher Education Deemed to be University, Vijayawada 520 007, India

[b]Department of Electronics and Communication Engineering, National Institute of Technology, Jamshedpur 831 014, India

Received: 27th May 2026; accepted: 1st September 2026

This work focuses on the development of a cylindrical gate-all-around junctionless transistor (CY-GAAJLT)-based photodetector for ultraviolet (UV) detection. To investigate the sensitivity of the proposed device under illuminated and dark conditions, comprehensive TCAD simulations have been performed. Zinc oxide (ZnO) is used as a transparent optical gate material in the proposed device structure to improve UV light interaction and detection capability. To optimize the sensitivity of the CY-GAAJLT structure, several device parameters were systematically tuned by analyzing the influence of the wavelength and intensity of the incident optical beam. The simulation results demonstrate that the proposed novel CY-GAAJLT structure achieves the highest subthreshold drain current at a wavelength of 350 nm, corresponding to the UV region of the electromagnetic spectrum due to effectively controlling of gate all around the channel. The results demonstrate that the proposed CY-GAAJLT structure is very sensitive to incident UV light, which makes it a viable option for low-power UV photodetector applications. Additionally, significant performance parameters of the CY-GAAJLT photodetector, such as quantum efficiency (QE) and responsivity (R), have been comprehensively investigated. The proposed device exhibits an internal quantum efficiency (QE_I) of 0.13 and an external quantum efficiency (QE_E) of 0.16 under an optical radiation intensity of 12 W/cm².

Keywords: Cylindrical gate all around junctionless transistor (CY-GAAJLT), Photodetectors, Zinc oxide (ZnO), Quantum efficiency

1 Introduction

In the recent years, considering the variety of different applications of UV Photodetectors such as inter-satellite communications, flame detection, missile launching system and harmful UV detection, a tremendous amount of endeavor have been made to develop new advance UV photodetectors[1,2]. Extensive investigations have been carried out on wide bandgap semiconductor materials such as ZnO, boron nitride (BN), and gallium oxide (Ga_2O_3) because of their excellent UV light detection capabilities[3-5]. Attribute to its wide and direct band gap of approximately 3.37 eV and huge excitation energy of about 60 meV[6,7], ZnO is considered as the potential metal oxide semiconductor material for the manufacturing of photodetectors to detect UV radiation[8]. Furthermore, ZnO is extremely appropriate for a wide range of optoelectronic applications due to its low fabrication expenses, biocompatibility, and highly tunable optical and structural properties, which contribute to enhanced sensitivity and strong noise immunity[9-11]. A ZnO gate layer was employed to facilitate UV absorption, while the proposed device exhibited enhanced sensitivity and responsivity under low intensity UV illumination[12]. Similarly, recent work on double-gate junctionless FETs has demonstrated their potential for low power UV photodetection, with the junctionless structure providing improved gate control and reduced leakage current[13]. Furthermore, deploying cylindrical gate all around (GAA) nanowire MOSFETs with dual metal gate stacking introduces a distinct operational advantage. By monitoring subthreshold conduction modulation rather than relying on conventional threshold voltage shifts, these cylindrical GAA structures achieve extraordinary photo to dark current ratios (I_{illum}/I_{dark}) alongside superior short channel effect (SCE) immunity under submicron optical excitation[14]. The sensitivity of a photodetector towards incident optical radiation is one of the key factors determining its performance[15].

*Corresponding author: E-mail: bbinay2010@gmail.com

Enhancement in photodetector sensitivity is largely associated with the reduction of OFF-state leakage current within the device structure[16]. Owing to their inherently low leakage current and superior subthreshold characteristics, junctionless transistors have attracted considerable research attention in recent years compared with conventional device structures such as MOSFETs and hetero/homo-junction diodes[17-20]. Several crucial design parameters control complete depletion at zero gate bias in a junctionless transistor[21,22]. Firstly, the semiconductor channel must be heavily doped to facilitate efficient current conduction. Secondly, the channel dimensions should be sufficiently narrow and thin to ensure complete depletion in the OFF-state condition. A nanowire GAA MOSFETs offer superior gate controllability, reduced leakage current, and improved scalability compared with conventional planar MOSFETs through appropriate optimization of the gate and channel dimensions[23,24]. Similarly, a ferroelectric GAA MOSFETs exhibit improved switching characteristics, reduced subthreshold swing, lower drain induced barrier lowering (DIBL), and enhanced immunity to short-channel effects[25]. For UV photodetection, such enhanced electrostatic control is particularly advantageous because it enables effective modulation of the channel conductivity in response to photogenerated carriers, thereby supporting improved photoresponse and suppression of unwanted leakage or dark current. Furthermore, the cylindrical GAA configuration provides an efficient channel gate interaction within a compact geometry, making it a suitable structure for high performance and scalable junctionless UV photodetectors.

In this work, the UV light detection capability of a cylindrical gate-all-around junctionless transistor (CY-GAAJLT) employing a transparent ZnO gate has been systematically investigated. To optimize the sensitivity and detection performance of the proposed device, key structural and material parameters, including oxide thickness, channel thickness, doping concentration, and minority carrier lifetime, have been carefully varied and analyzed.

2 Methods and Materials

2.1 Device Description

Figure 1 (a) illustrates the 3D schematic representation of the proposed cylindrical gate-all-around junctionless transistor (CY-GAAJLT) investigated in this study, whereas Fig. 1 (b) presents the corresponding 2-D cross sectional view of the cylindrical GAAJLT device structure. In Fig. 1(a), L_{ch} denotes the channel length, (r) represents the channel radius, T_{ox} corresponds to the thickness of the dielectric oxide layer (SiO_2), and L_g indicates the gate length. The different device parameters used during the simulation process are presented in Table 1. Here, the channel length is denoted by L_{ch}, the

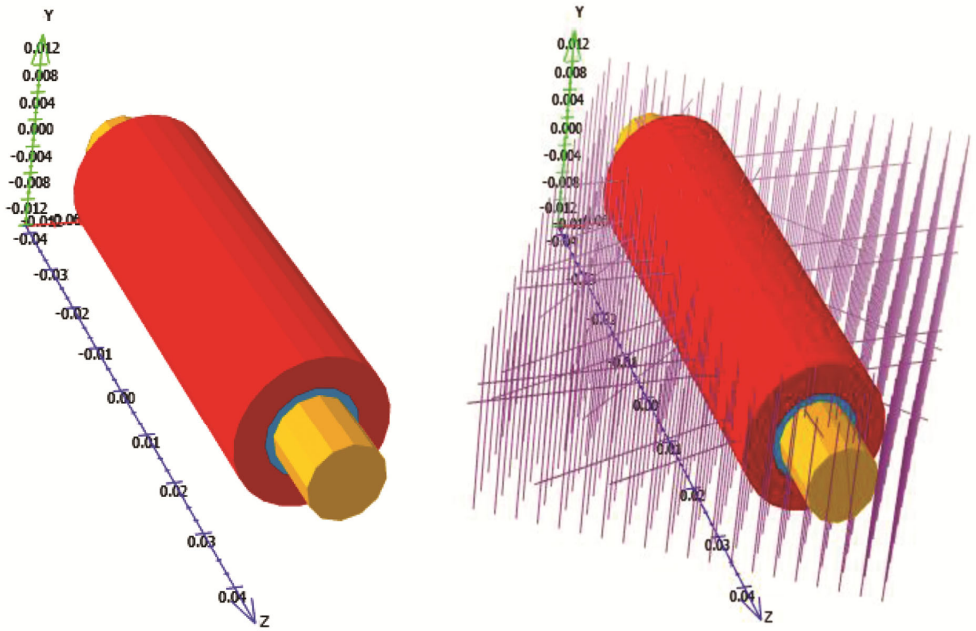

Fig. 1 — (a) CY-GAAJLT under dark condition; and (b) CY-GAAJLT under the optical illumination with different optical intensities

Table 1 — Device parameters employed for simulation

Symbol	Description	Value
L_{ch}	Channel Length (Si)	80 nm
L_g	Gate Length	60 nm
T_{ox}	Dielectric thickness (SiO_2)	1 nm
T_g	Gate Thickness	4 nm
r	Radius of channel	5 nm
T_{si}	Thickness of Channel (T_{si}=2R)	10 nm
N_a	Channel Doping	10^{19} per cm^3

channel radius by (r), the thickness of the dielectric oxide layer (SiO_2) by T_{ox}, and the gate length by L_g in Fig. 1 (a). Table 1 lists the different device parameters used throughout the simulation process.

2.2 Simulations and Physical Models

All the electrical and optical characteristics of the CY-GAAJLT have been obtained using the ATLAS TCAD-3D simulator[26]. To analyze the device performance under optical illumination, the BEAM statement available in the LUMINOUS-3D module has been employed, and the photogeneration rate has been calculated using the ray-tracing method. The incident optical beam is assumed to be normally incident on the gate surface in the LUMINOUS-3D simulation framework. Furthermore, the optical model accounts for reflection losses at the relevant material interfaces by incorporating the corresponding reflection coefficients into the photogeneration formulation. The BEAM statement enables precise control of various optical parameters, including the intensity, wavelength, and position of the incident optical beam. The dark characteristics of the CY-GAAJLT have been extracted by setting the beam intensity to zero.

To achieve accurate simulation results for the CY-GAAJLT, several physical models have been incorporated, including the Field-Dependent Mobility (FLDMOB) model, Band Gap Narrowing (BGN) model, and Shockley Read Hall (SRH) recombination model. The BGN model accounts for the bandgap narrowing effects occurring within the device, while the FLDMOB model describes the variation of carrier mobility under high electric field conditions. Furthermore, the carrier recombination mechanisms within the device are modelled using the SRH recombination model.

3 Results and Discussion

The I_d vs. V_{gs} characteristic curves of the CY-GAAJLT under dark conditions as well as under optical illumination at different optical intensities are depicted in Fig. 2. The plot demonstrates the variation of drain current (I_d) with gate-to-source voltage (V_{gs}) when the device is exposed to optical radiation of varying intensities at a fixed wavelength. In the proposed CY-GAAJLT structure, an increase in the intensity of the incident optical radiation enhances channel conduction, thereby resulting in a higher drain current due to effectively controlling of gate all around channel. Compared to the linear and saturation regions, the variation in drain current with optical intensity is found to be significantly more prominent in the subthreshold region[27], thereby demonstrating the suitability of the proposed device structure for UV photodetector applications operating in the subthreshold regime.

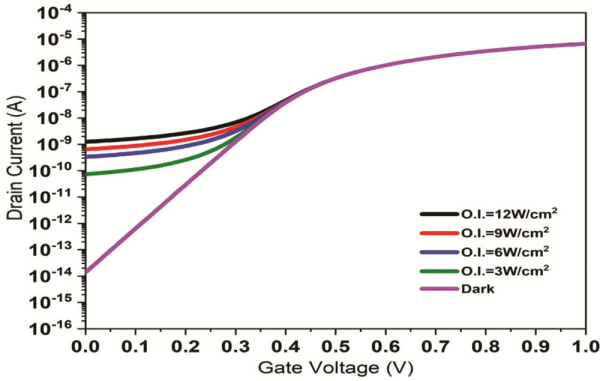

Fig. 2 — Presents the I_d vs V_{gs} characteristics of the CY-GAAJLT under different optional illumination intensities at V_{ds}=0.15°V,λ=350°

Furthermore, the thicknesses of the ZnO and SiO_2 layers have been minimized to ensure maximum penetration of the incident optical radiation into the channel region, thereby facilitating enhanced electron–hole pair (EHP) generation. The photogeneration rate (G_r) can be expressed using Eq. (1)[28].

$$G_r = \alpha I_0 \frac{h}{c\lambda}(1\text{-}R_1) \times (1\text{-}R_2) \times (1\text{-}R_3) \quad \ldots (1)$$

The Various coefficients involved in the above expression are summarized in Table 2.

Figure 3 illustrates the variation of (I_d) with respect to the incident optical wavelength under different optical illumination intensities. The plotted characteristics clearly indicate a substantial increase in (I_d) when the device is illuminated with wavelengths corresponding to the UV region of the electromagnetic (EM) spectrum. This behavior confirms the capability of the proposed structure to operate effectively as a UV photodetector.

Table 2 — Co-efficient of photo generation rate

α	Absorption co-efficient
h	Planks constant
c	Speed of light
I_0	Optical Intensity
R_1	Reflection co-efficient of Air/Gate interface
R_2	Reflection Co-efficient of Gate/SiO2 interface
R_3	Reflection Co-efficient of SiO2/Si Channel interface

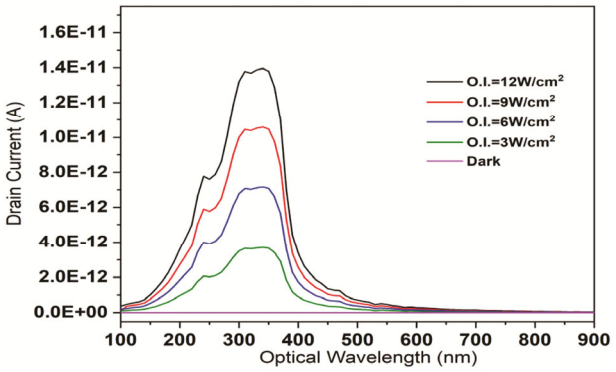

Fig. 3 — I_d vs Wavelength (λ) at Zero Gate biasing (V_{gs}=0), V_{ds} =0.15V at varying intensities

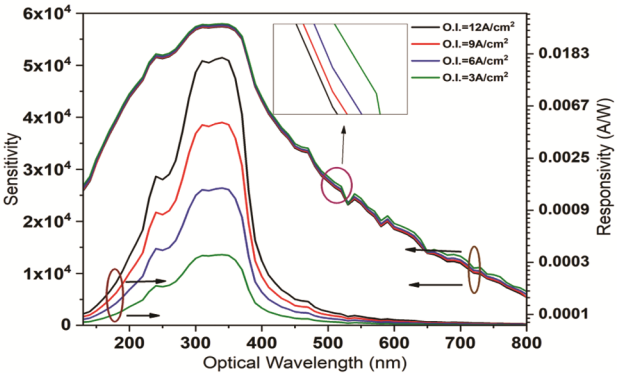

Fig. 4 — Sensitivity vs Optical Wavelength (λ) vs Responsivity at multiple intensities, V_{gs}=0V, V_{ds}=0.15V

Sensitivity and responsivity are the important parameters which define the efficiency of a photodetector. The expression depicted in Eq. (2) can be used to determine the sensitivity of the CY-GAAJLT[29].

$$\text{Sensitivity}=\frac{I_{light}-I_{dark}}{I_{dark}} \quad \ldots (2)$$

Figure 4 illustrates the dependence of the sensitivity and responsivity (R) of the CY-GAAJLT on the variation in the (λ) of the incident optical radiation. Figure 4 clearly demonstrates that the sensitivity of the CY-GAAJLT increases with increasing wavelength (λ) within the UV region. This behaviour can be attributed to the increased

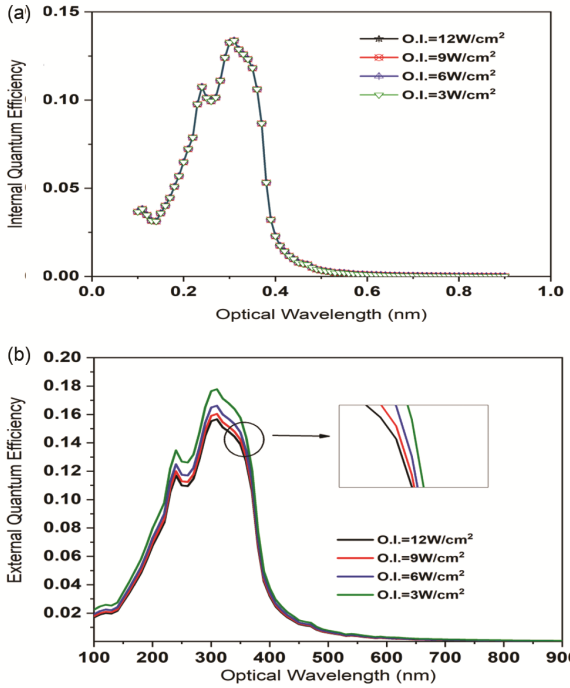

Fig. 5 — (a) QE_I vs Wavelength (λ), I_0=12W/cm^2, V_{ds}=0.15V,V_{gs}=0V, (b) QE_E vs Optical Wavelength (λ), V_{ds}=0.15V, V_{gs}=0V

absorption of optical radiation by silicon for wavelengths beyond 280 nm, owing to the corresponding incident photon energy (hc/λ), where (h) represents Planck's constant and (c) denotes the speed of light in vacuum[30]. The responsivity (R) of the proposed structure can be calculated using the expression given in Eq. (3)[31].

$$R=\frac{I_{light}-I_{dark}}{I_0 A} \quad . (3)$$

In this expression, (I_0) signifies the intensity of the incident optical radiation, whereas (A) indicates the illuminated area of the device. Quantum efficiency (QE) is another significant parameter commonly employed to assess the performance of a photodetector[32]. The quantum efficiency of a photodetector can be categorised into internal quantum efficiency (QE_I) and external quantum efficiency (QE_E), both of which can be calculated using the expressions given below[33,34].

$$QE_I=\frac{I_A}{I_S} \quad \ldots (4)$$

$$QE_E=\frac{I_D}{I_S} \quad \ldots (5)$$

Here, I_S, I_A, and I_D represent the available source current, available photocurrent, and dark current,

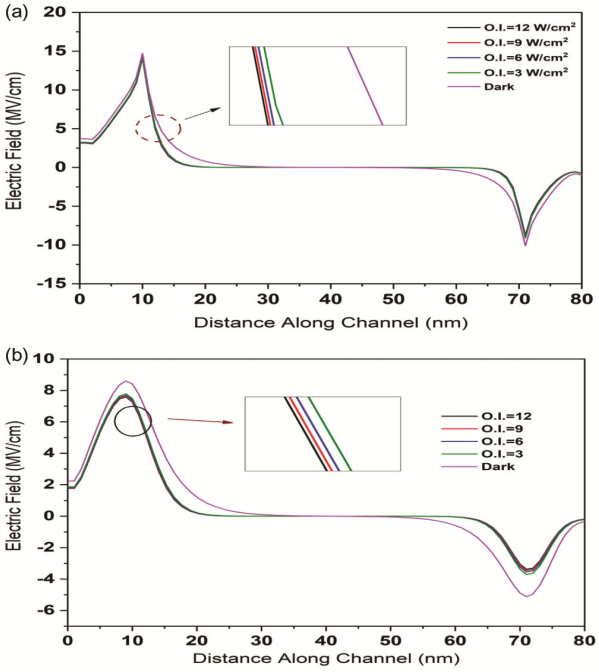

Fig. 6 — (a) E-Field vs distance along channel at the surface of the channel at V_{ds}=0.15V, λ=350nm, (b) illustrates the variation of electric field with distance along the center of the channel at $V_{ds} = 0.15$ Vand $\lambda = 350$ nm

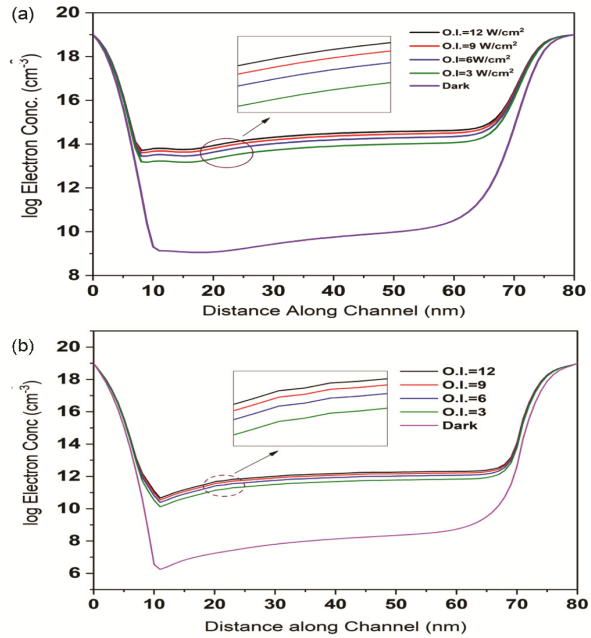

Fig. 7 — (a) Electron concentration at the center of channel at V_{ds}=0.15V, λ=350nm, (b) Electron concentration at the channel surface for V_{ds}=0.15V, λ=350 nm

respectively. Figure 5 (a) and (b) illustrate the variation of internal quantum efficiency and external quantum efficiency, respectively, as a function of the incident optical wavelength.

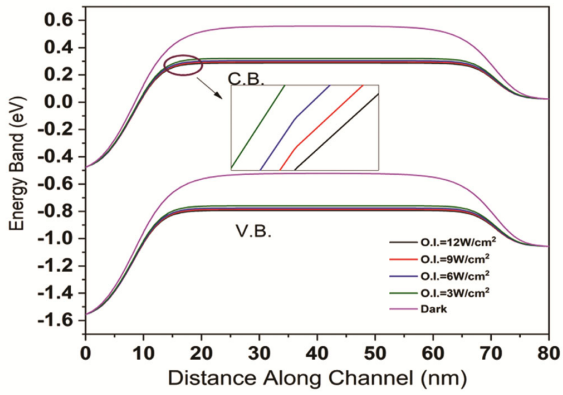

Fig. 8 — Energy band Diagram variation along the channel length at V_{ds}=0.15V, λ=350nm

The variations in (QE_I) and (QE_E) with respect to the incident optical wavelength are shown in Fig. 5 (a) and (b), respectively. It is clearly evident from the plotted characteristics that the (Q_E) gradually increases, attains its maximum value within the UV spectral region, and subsequently decreases with further increase in wavelength. This behavior confirms the effectiveness of the proposed CY-GAAJLT structure as a UV photodetector.

Furthermore, to analyze the static behavior of the proposed device, the structure has been symmetrically sliced along the *X–Y* plane, two cutlines have been taken along the channel length, with one passing through the center of the channel and the other located at the channel surface. The electric field variation along the channel length at the channel's surface and center is shown in Fig. 6 (a) and (b) respectively, under different optical illumination intensities. It has been observed that the electric field within the channel decreases with increasing incident optical intensity. Moreover, the electric field under illuminated conditions has been found to be lower than that observed under dark conditions.

As a consequence of the reduced electric field under illuminated conditions at the center of the channel, the electron concentration is observed to be higher at the centre of the channel in comparison with the channel surface, as depicted in Fig. 7 (a) and (b). Furthermore, a lower electric field near the drain side is essential for achieving reduced OFF-state current[35].

Figure 8 illustrates the energy band diagram of the CY-GAAJLT structure under dark conditions as well as under optical illumination at different intensities. Upon exposure to optical radiation, the energy bands undergo bending, which leads to channel activation and consequently facilitates current conduction through the device[36].

Table 3 — Comparative performance evaluation of ZnO photodetector structures

Channel material	I_{dark}	I_{photon}	Responsivity (A/W)	Sensitivity	Ref
ZnO	8.9×10^{-6}	4.3×10^{-7}	0.047	-	[38]
Au on ZnO	3.2×10^{-9}	4.3×10^{-6}	0.89	1.3×10^{3}	[39]
ZnO	-	-	48.8	1.7×10^{4}	[40]
Pt on ZnO	2.2×10^{-9}	4.3×10^{-6}	-	-	[41]
ZnO	-	-	5.6	5.5×10^{3}	[42]
ZnO	4.5×10^{-8}	1.0×10^{-5}	27	2.3×10^{2}	[43]
ZnO	1.5×10^{-14}	7×10^{-6}	0.02	~5.8 × 10^{4}	Proposed work

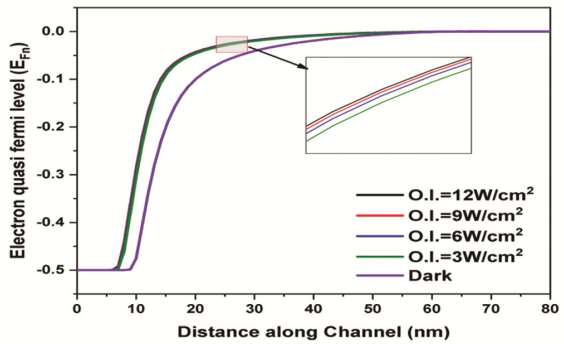

Fig. 9 — Electron quasi fermi level (E_{Fn}) variation along the channel length at V_{ds}=0.15V, λ=350nm

Figure 9 illustrates the variation of the electron quasi-Fermi level (E_{Fn}) along the channel length of the CY-GAAJLT structure. It is observed that the (E_{Fn}) level shifts towards the left with an increase in the intensity of the incident optical radiation. This behaviour occurs due to the increased generation of electron-hole pairs (EHPs) under optical illumination, which induces energy band bending and consequently results in the leftward shift of (E_{Fn})[37].

A comparative evaluation of the proposed ZnO based UV photodetector with previously reported photodetector structures is represented in Table 3. The performance characteristics of conventional ZnO photodetectors, as well as Au and Pt functionalized ZnO structures, have been reported. These studies provide a basis for evaluating important photodetector parameters, including dark current, photocurrent, responsivity and sensitivity[38-43]. The proposed device exhibits a responsivity of 0.02 A/W and a sensitivity of ~5.8 × 10^{4} demonstrating its potential for UV photodetection applications.

Furthermore, as the incident optical radiation falls on the gate surface, additional (EHPs) are generated. Since the channel is heavily doped with n-type impurities, the channel potential exhibits significant variation under optical illumination, leading to a substantial increase in the illuminated (I_d) compared

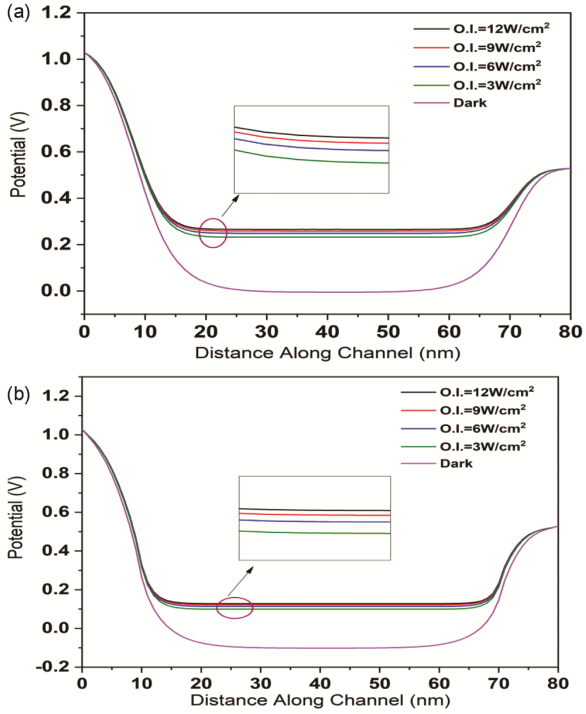

Fig. 10 — (a) Potential variation along the channel length at center of the channel when Vds=0.15V, λ=350nm, (b) Potential variation along the channel length at surface of the channel at Vds=0.15V, λ=350nm

with the dark current[44]. Figure 10 (a) and (b) depict the variation of channel potential with respect to distance along the channel length (L_{ch}) at the centre and surface of the channel, respectively. The Table III compares the reported electrical and photoresponse characteristics of ZnO based UV photodetectors with those of the proposed device. The proposed ZnO photodetector exhibits a very low dark current, high sensitivity of ~5.8×10^{4} demonstrating its potential for UV detection.

4 Conclusion

In this work, a cylindrical gate-all-around junctionless transistor (CY-GAAJLT)-based UV

photodetector has been simulated and analysed with respect to various performance parameters, including sensitivity and responsivity (R). Based on the obtained simulation results, it has been verified that the proposed device structure, employing ZnO as the gate material and SiO_2 as the gate dielectric material, exhibits high sensitivity of (~5.8×10^4) towards optical radiation in the UV spectral region, thereby demonstrating its suitability for UV photodetector applications. The CY-GAAJLT exhibits enhanced photocurrent under UV illumination, along with low dark current and reduced threshold voltage, supporting low power subthreshold operation. The device achieves a responsivity of ~0.02 A/W and a maximum external quantum efficiency of 0.16 (~16 %) at ~300 nm, demonstrating its potential for efficient, low power UV photodetection.

References

1 Xu X, Xu C & Hu J, *J Appl Phys*, 116 (10) (2014) 103105.
2 Lausecker C, Baillard A, Appert E & Consonni V, *Electron*, e70040 27 (2026) 70040.
3 Aldalbahi A & Feng P, *IEEE Trans Electron Devices*, 62 (6) (2015) 1885.
4 Zhang Q, Jie J, Diao S, Shao Z, Zhang Q, Wang L, Deng W, *et al*., *ACS Nano*, 9 (2) (2015) 1561.
5 Xu J, Zheng W & Huang F, *J Mater Chem C*, 7 (29) (2019) 8753.
6 Kumar B B, Tiwari P K, Dubey S & Singh K, *Micro Nanostruct*, 164 (2022) 107122.
7 Kumar B B, Bhowmik B, Singh A P, Jit S & Singh K, *Appl Phys A*, 130 (5) (2024) 308.
8 Boruah B D, *Nanoscale Adv*, 1 (6) (2019) 2059.
9 Kumar B B, Kavi K K, Raut P, Tripathi B M M & Singh K, *Micro Nanostruct*, 8 (2026) 208844.
10 Raut P, Nanda U, Panda D K & Hsu C-C, *2023 3rd International Conference on Artificial Intelligence and Signal Processing (AISP)* (IEEE) 2023, 1.
11 Kumar B B, Raj S, Singh K, Kavi K K & Kumar S, *Micro Nanostruct*, 206 (2025) 208248.
12 Choi Y, Kim D, Baek J, Kim H Y, Kim Y, Park S-H K, Shin M & Cho B J, *IEEE Trans Electron Devices* 73 (3) (2026) 1455.
13 Rani D, Raikwal P & Dutta K, *2026 IEEE International Conference on Interdisciplinary Approaches in Technology and Management for Social Innovation (IATMSI)* (IEEE) 2026, 1.
14 Sharma S K, Kumar P, Raj B & Raj B, *Silicon*, 14 (7) (2022) 3535.
15 Jain A, Sharma S K & Raj B, *Eng Sci Technol Int J*, 19 (4) (2016) 1864.
16 Park K, Lee J-S, Sung M-Y & Kim S, *Jpn J Appl Phys*, 41 (12) (2002) 7317.
17 Colinge J-P, Lee C-W, Afzalian A, Akhavan N D, Yan R, Ferain I, Razavi P *et al*., *Nat Nanotechnol*, 5 (3) (2010) 225.
18 Lime F, Moldovan O & Iñiguez B, *IEEE Trans Electron Devices*, 61 (9) (2014) 3036.
19 Baidya A, Baishya S & Lenka T R, *Mater Sci Semicond Process*, 71 (2017) 413.
20 Colinge J P, Lee C-W, Akhavan N D, Yan R, Ferain I, Razavi P, Kranti A & Yu R, *Semiconductor-on-Insulator Materials for Nanoelectronics Applications* (Springer, Berlin, Heidelberg) 2011, 187.
21 Kumari V, Gupta M & Saxena M, *IEEE Trans Electron Devices*, 68 (6) (2021).
22 Mondal P, Ghosh B, Bal P, Akram M W & Salimath A, *Appl Phys A*, 119 (1) (2015) 127.
23 Raut P, Nanda U & Panda D K, *Nanodevices for Integrated Circuit Design* (2023) 93.
24 Kumar B B, Dubey S, Jit S & Singh K, *Micro Nanostruct*, 189 (2024) 207796.
25 Raut P, Nanda U & Panda D K, *Phys Scr*, 97 (10) (2022) 105809.
26 *ATLAS User's Manual 3-D Device Simulator*, SILVACO International, Version 5.14.0.R (2010).
27 Jahromi H D, Zeiri N & Lotfiani A, *J Sci Adv Mater Devices*, 10 (3) (2025) 100891.
28 Kumari V, Gupta M & Saxena M, *IEEE Trans Electron Devices*, 68 (6) (2021) 2841.
29 Bafghi Z G & Manavizadeh N, *Superlattices Microstruct*, 122 (2018) 18.
30 Sze S M, *Physics of Semiconductor Devices*, 2nd edn (Wiley, Hoboken, NJ) 1981, 804.
31 Lee E, Moon D, Yang J H, Lim K S & Choi Y K, *IEEE Electron Device Lett*, 30 (5) (2009) 493.
32 Saxena P K & Chakrabarti P, *Infrared Phys Technol*, 52 (2009) 196.
33 Lal R K, Jain M, Gupta S & Chakrabarti P, *Infrared Phys Technol*, 44 (2003) 125.
34 Sharma S, Sumathi A & Periasamy C, *IETE Tech Rev*, (2016).
35 Zhang J, Wu X, Lin H, Wang L, Zhang H, Wang F, Li M et al., *IEEE Trans Electron Devices*, 71 (10) (2024) 6281.
36 Xie C & Yan F, *Small*, 13 (43) (2017) 1701822.
37 Yang G, Li J, Wu M, Yu X & Yu J, *Adv Electron Mater*, 9 (10) (2023) 2300340.
38 Kim J-H, Choi J, Na H & Lee S-N, *Adv Mater Interfaces*, 10 (17) (2023) 2300176.
39 Chu Y-L, Liu Y-H, Chu T-T & Young S-J, *IEEE Sens J*, 22 (6) (2022) 5644.
40 Debnath S, Ghosal S, Meyyappan M & Giri P K, *Flex Print Electron*, 9 (3) (2024) 035005.
41 Young S-J & Liu Y-H, *IEEE J Electron Devices Soc*, 9 (2021) 265.
42 Khanzode P M, Shaikh S J, Halge D I, Thabit M Y H, Rahman A B U, Narwade V N, Dahiwale S S & Bogle K A, *ACS Appl Eng Mater*, 3 (6) (2025) 1678.
43 Zheng M, Gui P, Wang X, Zhang G, Wan J, Zhang H, Fang G, Wu H, Lin Q & Liu C, *Appl Surf Sci*, 481 (2019) 437.
44 Simone G, Dyson M J, Meskers S C J, Janssen R A J & Gelinck G H, *Adv Funct Mater*, 30 (20) (2020) 1904205.